Kinetics and Catalysis, Vol. 46, No. 3, 2005, pp. 319–327. Translated from Kinetika i Kataliz, Vol. 46, No. 3, 2005, pp. 344–353.

Autoignition of a Lean Propane–Air Mixture at High Pressures

V. P. Zhukov, V. A. Sechenov, and A. Yu. Starikovskii

Moscow Institute of Physics and Technology, Dolgoprudnyi, Moscow oblast, 141700 Russia

e-mail: victorzhukov@mail.ru

Received November 20, 2003

Abstract—Ignition delay time behind a reflected shock wave is measured for a lean propane–air mixture with an equivalence ratio of $\varphi = 0.5$ in wide temperature and pressure ranges (T = 880–1500 K, P = 2–500 atm). Ignition-delay activation energy data obtained in this study are compared with earlier data. A detailed kinetic model is constructed for hydrocarbon ignition, which includes ignition mechanisms for low, high, and intermediate (1000–1200 K) temperatures. Each of the mechanisms is analyzed. The effect of pressure on the mechanism of autoignition is demonstrated.

Most of the previous reports relevant to the subject at hand deal with the autoignition of C_3H_8–O_2–Ar mixtures containing 97–99% Ar [1–5]. Ignition delay time (τ) data were acquired at different pressures and mixture compositions and, as a consequence, vary in a wide range. The temperature dependences of τ observed in those experiments fit the Arrhenius law well; therefore, they can be conveniently compared in terms of the correlation formula

$$\tau = A\exp(E_a/RT)[C_3H_8]^\alpha[O_2]^\beta[\mathrm{Ar}]^\gamma, \qquad (1)$$

where E_a is the apparent ignition-delay activation energy; A is the preexponential factor; and α, β, and γ are fitted coefficients. The results of the above-mentioned studies suggest that E_a is independent of temperature between 1250 and 2200 K, of pressure between 0.75 and 10 atm, of equivalence ratio between 0.125 and 2.0, of the nature of the diluent gas, and of diluent concentration in the range 97–99%. The E_a value for C_3H_8–O_2–Ar mixtures (56.5 kcal/mol) is close to the value observed for similar methane-containing mixtures (54.5 kcal/mol) [1].

There have been studies on the ignition of C_3H_8–O_2–Ar (N_2) mixtures similar in composition to typical fuel–air mixtures (containing ~77% diluent gas) at temperatures above 1100 K and pressures up to 10 atm [3–7]. Ignition delay time was measured for propane–air, primarily lean, mixtures in an intermediate temperature range of 850–1280 K and at high pressures of 5 to 40 atm [6]. It was found that, as the temperature is lowered from 1280 to ~1000 K, E_a for the $C_3H_8 : O_2 : N_2$ = 2.1 : 20.6 : 77.3 mixture decreases by a factor of 2, specifically, from 26 to 13 kcal/mol. This large decrease in E_a was not detected earlier because of difficulties in shock-tube investigation of autoignition at 700–1000 K: it is only at high pressures that the ignition delay time for most fuel mixtures at temperatures around 1000 K is within the measurement range.

The marked decrease in E_a at $T \approx 1000$ K for undiluted lean propane–air mixtures is not unexpected. There has been a report on oxidation in a propane–air mixture with an equivalence ratio of $\varphi = 0.4$ in a flow reactor at T = 650–800 K and P = 10–15 atm [8]. The residence time of this mixture was 198 ms. Between 720 and 780 K, the extent of chemical reaction (estimated from the concentrations of oxidation products at the reactor outlet) showed a negative temperature coefficient (NTC); that is, it decreased with increasing temperature. The reaction mechanism suggested by the authors of that study [8] provides a plausible explanation for the experimental data: the temperature coefficient is negative because temperature variations cause displacement of the equilibria in the $\dot{C}_3H_7 + O_2$ and $C_3H_7O_2H + O_2$ reactions. Therefore, between the $T >$ 1200 K region, where the activation energy is high, and the $T <$ 1200 K region, where an NTC is observed, there must be a region where the activation energy takes intermediate values. This region was explored in [6]. However, most of the experimental data presented in that report was collected at pressures below 10 atm and the kinetic model suggested by the authors led to an ignition delay time longer than was experimentally observed. The pressure dependence of τ and the mechanism of propane oxidation in the temperature range examined were not studied. At the same time, mechanisms have been suggested for propane oxidation outside the intermediate temperature range. For example, a detailed mechanism has been reported for the oxidation of C_2 and C_3 hydrocarbons [9]. This mechanism has been experimentally confirmed by oxidation, ignition, and flame structure studies on hydrogen, carbon monoxide, formaldehyde, methanol, methane, ethane, propane, and their mixtures. For the propane–air mixture, the observed velocity of laminar flame at T = 298 K and P = 1 atm was compared with the model value.

0023-1584/05/4603-0319 © 2005 MAIK "Nauka/Interperiodica"

Experimental investigation of NO reduction with propane at 1 atm and a propane concentration of 0.2–0.3% in the temperature range 1150–1400 K [10] demonstrated that the authors' kinetic model is in fair agreement with experimental data. This model includes the mechanism of oxidation of C_1 and C_2 hydrocarbons that was earlier verified by studying the effects of ethane, ethylene, and methane on NO concentration.

The variation of apparent ignition-delay activation energy between 1000 and 1200 K is typical of the oxidation of not only propane but also other alkanes. Peterson *et al.* [11] measured ignition delay time for CH_4–O_2–diluent (Ar, He, N_2) mixtures in the temperature range 1040–1600 K and in the pressure range 35–260 atm at low diluent concentrations of 66–80% and $\varphi = 0.4$, 3, and 6. For methane-rich mixtures, as the temperature was decreased to ~1300 K, the activation energy fell from 32.7 to 19 kcal/mol. Later, Peterson *et al.* [12] formulated a kinetic model known under the name RAMEC, which is capable of reliably predicting ignition delay time over the temperature range 1040–1500 K. This model includes the well-known mechanism GRI 1.2 [13] supplemented with reactions involving $^{\cdot}CH_3O_2$, CH_3O_2H, C_2H_5O, $^{\cdot}C_2H_5O_2$, and $C_2H_5O_2H$. The fact that activation energy decreases as the temperature is lowered is explained by the existence of extra branching channels at $T < 1100$ K:

$$^{\cdot}CH_3O_2 + {}^{\cdot}CH_3 \longrightarrow 2CH_3O^{\cdot}, \qquad \text{(I)}$$

$$H_2O_2(+M) \longrightarrow {}^{\cdot}OH + {}^{\cdot}OH(+M). \qquad \text{(II)}$$

The ignition of lean methane–air mixtures behind a reflected shock wave is considered in greater detail in [14, 15]. Ignition-delay activation energy decreases from 44 kcal/mol at 3–4 atm and 1550–1650 K to 24 kcal/mol at 400–500 atm and 1200–1400 K. In an earlier publication [16], we reported ignition delay time behind a reflected shock wave for a lean *n*-hexane–air mixture in the temperature range 820–1380 K and the pressure range 13–220 atm. At temperatures of 1000–1090 K and pressures above 60 atm, the temperature derivative of τ is close to zero. Our experimental data are in good agreement with data calculated using the kinetic model reported in [17]. That model is designed for *n*-heptane oxidation. It was developed step-by-step to mediate between light and heavy hydrocarbons. It includes the above-mentioned mechanism of propane oxidation [8], which implies the existence of an NTC region. Its latest version [18] describes the oxidation of alkanes up to octane. The mechanism reported in [17] was experimentally verified against *n*-heptane oxidation in a wide range of thermodynamic parameters: pressure, 1–42 atm; temperature, 550–1700 K; $\varphi = 0.3$–1.5; and diluent (nitrogen or argon) concentration, 70–99%. Data obtained in shock tubes, rapid-compression machines, and flow reactors were used in verification. This mechanism provides very precise estimates for the ignition delay time of *n*-heptane–air mixtures at temperatures of 700–1300 K and pressures up to 42 atm. Ignition delay time behind the shock wave was measured for these mixtures [19, 20]. Between 750 and 950 K, the temperature dependence of τ is characterized by a negative temperature coefficient. According to the above-mentioned model [17], this is due to mechanistic changes: at low temperatures, alkylketyl hydroperoxides participate actively in chain branching. The detailed mechanism of this process includes 2450 reactions and 550 components. A drawback of this mechanism is that the methane oxidation submechanism fits experimental data worse than any other CH_4 oxidation mechanism [12, 21, 22].

The purpose of our work was to obtain experimental data on the autoignition of a lean propane–air mixture and to construct a kinetic model explaining the variation of ignition delay time in a wide range of process parameters.

EXPERIMENTAL

Measurements were made behind a shock wave in a high-pressure shock tube. Shock tubes are perfect for combustion studies at high pressures and residence times of 2–3 ms for the following reasons: (1) the walls and windows of a tube are exposed to high pressures and temperatures only for a short time, (2) typical combustion temperatures of 1000–2000 K are easily attainable behind a reflected shock wave and are reproducible, (3) gas parameters behind the shock wave can easily be deduced from the initial gas parameters and the velocity of the shock wave, (4) the gas behind the shock wave is almost motionless and homogeneous, and (5) modern optical spectroscopic methods can be employed in kinetic studies. The main parameter measured in shock tubes is ignition delay time (induction period), which is the time interval between the instant the fuel mixture is heated by the shock wave and the instant a high conversion rate is reached.

Measurements behind a reflected shock wave can be made only over a limited period of time [23]. In our study, this period was no longer than 350 μs. A temperature interval of $\Delta T \approx 200$ K corresponded to this period at a fixed pressure. The interval ΔT can be markedly extended to lower temperatures by raising the pressure of the fuel mixture. We measured ignition delay time at pressures up to 500 atm, and the mixture temperature was varied between 880 and 1550 K.

The shock tube, with an inner diameter of 45 mm, was stainless steel. Its high-pressure section was 0.7 m long, and its low-pressure section was 3.2 m in length. The sections were separated by an auxiliary dual-diaphragm chamber. The diaphragms broke once the gas pressure in the high-pressure section reached a preset value. A specially designed pneumatic pump allowed operation at a pushing gas pressure up to 1000 atm. The gaskets used in the shock tube were made of copper, and the optical windows were sapphire. This technique

made possible kinetic studies behind reflected shock waves at pressures up to ~1000 atm.

The pushing gas was helium. The fuel–air mixture consisted of 98% dried air and 2% propane–butane mixture ($\varphi \approx 0.5$). The composition of the propane–butane mixture was determined by gas chromatography. The composition of the reaction mixture could very precisely be represented as $C_3H_8 : C_4H_{10} : O_2 : N_2 : Ar = 1.7 : 0.3 : 20.5 : 76.7 : 0.8$. After preparation, the mixture was left to stand for 48 h for complete mixing.

Gas pressure and temperature behind the reflected shock wave were calculated using the one-dimensional theory of ideal shock tubes under the assumption of complete vibrational relaxation, neglecting the chemical reactions. Since the ignition of saturated hydrocarbons is characterized by a high activation energy, the reaction rate behind the incident shock wave is much lower than the reaction rate behind the reflected wave. The ignition delay time under the "hottest" conditions attainable behind the incident wave was longer than 1 ms, while the instants the incident wave and the wave reflected from the tube end passed through the measurement cross section were separated by less than 30 μs. The assumption that the chemical reactions "are frozen" is confirmed by emission and absorption spectroscopic data, which demonstrate that there is no ignition behind the incident shock wave.

If the gas pressure behind the reflected wave exceeded 200 atm, the thermodynamic parameters of the mixture were calculated using the van der Waals equation. In these calculations, we used observed values of initial mixture pressure and temperature as well as wave velocities extrapolated to the tube end with allowance made for damping. Shock wave velocity was measured by the two-base schlieren method [24] with an accuracy of 1%. The corresponding uncertainties in gas temperature and pressure behind the shock wave were 1.3 and 2.7%, respectively.

Because of the strong temperature dependence of hydrocarbon oxidation rate, the error in temperature estimation behind the reflected shock wave causes a large error in ignition delay time. The actual velocity of the reflected shock wave and the thermodynamic parameters of the medium behind this wave are somewhat different from the corresponding values calculated without considering the effect of boundary layers [23]. However, at high pressures (3–500 atm) and short dwell times (<400 μs), the effects of nonideality can be neglected [25, 26].

Autoignition was watched through the side wall of the shock tube at a distance of 7 mm from the tube end. Ignition delay time was determined by time-resolved UV emission spectroscopy and IR absorption diagnostics. The UV emission system consisted of an MUM grating monochromator and an FEU-100 photomultiplier. Using this system, we studied the profile of radiation from the electronically excited radical $^{\cdot}OH$ ($A^2\Sigma^+ \longrightarrow X^2\Pi$ transition) at $\lambda = 309$ nm. The time-resolved emittance profile behind the shock wave is shown in Fig. 1. An absorption diagnostic system consisting of a He–Ne infrared laser ($\lambda = 3.3922$ μm) and a PbSe photoconductive cell was used along with the emission technique. By measuring absorbance at $\lambda = 3.3922$ nm, which was due to the asymmetric mode ν_3 of the CH_3 group, it was possible to monitor the propane concentration in the measurement cross section. The instant the incident or reflected wave passed through the measurement cross section was indicated by an increase in the absorption of radiation from the He–Ne laser. The time-resolved absorbance profile behind the shock wave is also shown in Fig. 1. The jumps of absorbance, which are due to gas density increasing behind the shock front, clearly indicate the instants the incident and reflected waves pass through the measurement cross section ($t = 0$ is the time point at which the reflected wave arrives at the measurement cross section). After an induction period, absorbance falls abruptly, indicating ignition and a decrease in the concentration of the compounds containing the CH_3 group. Ignition delay time was determined as the time interval between the instant the reflected wave passed the measurement cross section and the time point at which the emission from $^{\cdot}OH$ peaked (Fig. 1). A sketch of the shock tube and a detailed description of the autoignition detection procedures are presented elsewhere [14].

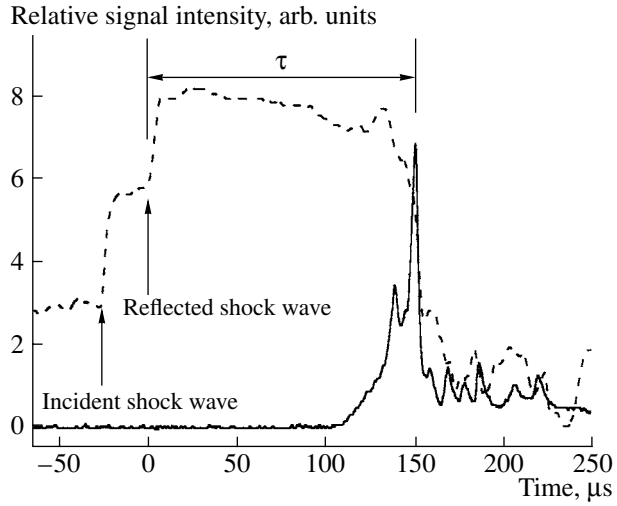

Fig. 1. Determination of ignition delay time using absorption and emission diagnostics. The dashed line is the absorption profile, and the solid line is the emission profile. $P = 19.7$ atm, and $T = 1247$ K.

When measuring the induction period by observing autoignition through the side wall of the tube, one should take into account that τ is affected by autoignition in regions that are nearer to the tube end than the measurement cross section [25]. In earlier studies [7, 11], ignition delay time for methane–air and *n*-hep-

Table 1. Ignition delay time data measured for a propane (2%)–air mixture

P, atm	T, K	t_{exp}, μs	Error, μs	P, atm	T, K	t_{exp}, μs	Error, μs	P, atm	T, K	t_{exp}, μs	Error, μs
3.63	1426	39	3	25.4	1301	71	3	67	1246	65	4
3.71	1450	34	3	24.7	1180	285	15	65	1222	78	4
3.93	1249	264	10	25.3	1244	128	6	66	1132	173	10
3.90	1259	229	12	26.0	1237	126	7	65	1134	166	8
2.16	1339	147	15	24.2	1596	10	3	67	1109	216	3
5.01	1524	15	3	19.9	1363	44	3	64	1188	99	3
4.66	1471	21	4	20.5	1425	23	3	211	1220	22	3
4.45	1272	223	20	19.3	1398	28	3	209	1123	57	3
4.38	1393	55	6	19.4	1283	106	8	207	1043	167	5
4.41	1324	131	3	21.3	1318	60	3	212	1023	180	4
4.77	1353	95	3	19.7	1247	153	7	207	1084	87	4
4.92	1501	17	7	17.7	1409	25	3	209	1164	45	3
10.00	1533	15	3	57	1344	21	3	487	1033	45	5
7.01	1538	11	3	58	1386	12	3	498	973	86	5
6.87	1332	153	6	53	1286	48	6	505	930	137	·
8.20	1552	10	3	59	1282	48	4	507	881	250	3
9.40	1517	12	3					493	1098	23	7

tane–air mixtures was simultaneously measured at the tube end and at a distance of 20 mm from the end. It was found that τ at the distance 20 mm is shorter by 20–45 μs than τ at the tube end. That is, the mixture behind the reflected shock wave ignites sooner at the tube end. On ignition, the mixture expands and displaces the gas away from the tube end. Furthermore, it promotes ignition in the adjacent cross section. As a consequence, the velocity of the combustion wave is higher than the velocity of the reflected shock wave. Here, we report τ data measured at a distance of 7 mm from the tube end. At this distance, applying a correction for the development of gas dynamic processes near the tube end changes τ by 7 ± 2 μs. Corrected ignition delay time data for a lean propane–air mixture are listed in Table 1.

CONSTRUCTION OF A MODEL

The adequacy of autoignition mechanisms was evaluated in terms of the best fit to experimental data obtained at $T \approx 1100$ K. The RAMEC mechanism most exactly describes the autoignition of methane–air mixtures at high pressures; however, it applies only to C_1 and C_2 hydrocarbons. Furthermore, recombination can take place at high reactant concentrations; therefore, when modeling the autoignition of propane–air and butane–air mixtures, it is necessary to take into account the reaction involving heavier hydrocarbons. This is the reason why the RAMEC mechanism of methane oxidation was supplemented with an oxidation mechanism for C_2–C_7 hydrocarbons [17]. However, the latter mechanism includes the processes occurring in the C_1–H–O system, thus leading to needless duplication of RAMEC reactions. This problem was solved by eliminating the duplicated reactions from the resulting reaction network, favoring RAMEC reactions. A similar procedure was used to avoid the duplication of thermodynamic data. The mechanism thus constructed includes 549 components and 2518 reactions.

The sensitivity of the model was analyzed using the SENKIN software package [27]. This package calculates the $dT(t)/dk_i$ derivatives, where k_i is the rate constant of the ith reaction under adiabatic conditions at a constant pressure. Next, it sums $dT(t)/dk_i$ values calculated at regularly spaced time points:

$$W_i = \sum_{t=0}^{t=\tau} dT(t)/dk_i. \quad (2)$$

In this summation, the induction period was set to be equal to the time taken by the mixture to heat up to the temperature 500 K above the initial temperature. The calculated integral coefficients characterizing the sensitivity of mixture temperature to reaction rate constants (W_i) were normalized to the sum taken over all reactions. The difference between W_i thus calculated and $d\tau/dk_i$ calculated for the RAMEC mechanism [12] does not exceed 10%. The effect of the rate constant of the ith reaction on ignition delay time can be evaluated using data presented in Fig. 2. The instant the concentration of reaction products (H_2O and CO_2) reaches half its ultimate value roughly coincides with the peak point of heat evolution. The rate of the chemical reactions increases many times in a short time interval (τ_{reac}), within which most of the fuel burns out and most

of the heat of reaction is released. The difference between induction periods determined using different criteria (change in pressure or temperature or a chemiluminescence peak) is close to the τ_{reac} value, which is much smaller than the induction period itself: $\tau_{reac}/\tau \leq 0.1$.

For a more precise description of experimental data, we optimized the mechanism considered. The original mechanism precisely predicts ignition delay time for $T = 1200$–1400 K. For $T = 1000$–1200 and 900–1000 K, it leads to overestimated and underestimated τ values, respectively. This misfit is observed between 60 and 500 atm. When selecting a reaction for optimization, we used the following criterion: the calculated ignition delay time must be sensitive to the rate constant of this reaction in the misfit region and depend only slightly on this rate constant in the close-fit region. Rate constants involved in the RAMEC mechanism were not changed. Sensitivity analysis demonstrated that, around 800 K, the induction period is determined by the rate of ketyl hydroperoxide decomposition, which is the main branching reaction at low temperatures. The rate constant of ketyl hydroperoxide decomposition in the mechanism suggested in [17] was decreased by a factor of 5. Between 1000 and 1100 K, a significant role in branching is played by the decomposition of alkyl hydroperoxy radicals that have resulted from alkyl peroxide isomerization. The rate constant suggested in [17] for this isomerization reaction (Table 2) was also decreased by a factor of 5. Starting at a higher temperature of 1100–1200 K, an important role in chain branching is played by the propane dehydrogenation reaction involving the $HO_2^{\cdot}$ radical. The optimization that we carried out resulted in a much better agreement between calculated and observed τ data in the temperature range 800–1100 K.

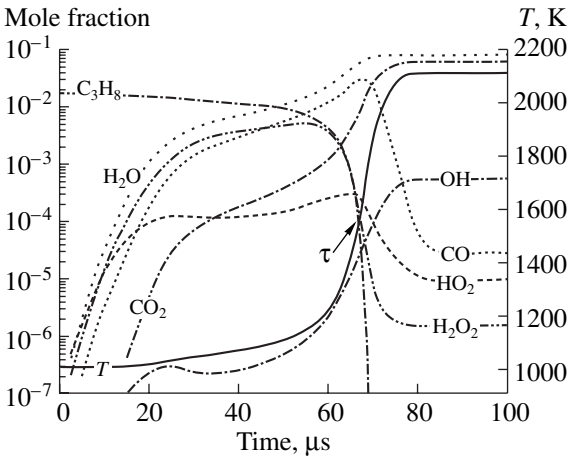

Fig. 2. Profiles of temperature and of the concentrations of the main components for a lean ($\varphi = 0.5$) propane–air mixture at $P = 500$ atm and an initial temperature of 1000 K as calculated using the kinetic model.

In the linear approximation, the sensitivity coefficient W_i is independent of the rate constant of the reaction. As is clear from the data listed in Table 3, optimization had only a slight effect on the sensitivity of ignition delay time to reaction rate constants (W_i data). The main result of optimization is a more important role of ketyl hydroperoxide formation and decomposition at $T = 1000$–1200 and 800–1000 K, respectively. Both before and after optimization, τ between 1000 and 1200 K is determined by the formation, accumulation, and subsequent decomposition of hydrogen peroxide.

In Fig. 3, we compare the observed τ data with the τ data calculated using our kinetic model. The observed and calculated data are in good agreement throughout the temperature and pressure ranges examined ($T = 800$–1500 K and $P = 5$–500 atm), including pressures

Table 2. Reactions optimized in the kinetic model and optimum parameters for reaction rate calculations

No.	Reaction		A	E, kcal/mol	X
1	$C_3H_8 + {}^{\cdot}HO_2 \longrightarrow {}^{\cdot}CH_2\text{–}C_2H_5 + H_2O_2$	chain branching ($T = 1000$–1200)	4.2×10^{13}, $cm^3\ mol^{-1}\ s^{-1}$	20.4	2.5
2	$C_3H_8 + {}^{\cdot}HO_2 \longrightarrow CH_3\text{–}{}^{\cdot}CH\text{–}CH_3 + H_2O_2$	chain branching ($T = 1000$–1200)	1.4×10^{13}, $cm^3\ mol^{-1}\ s^{-1}$	17.7	2.5
3	${}^{\cdot}C_3H_7O_2 = HOOCH_2\text{–}{}^{\cdot}CHCH_3$	ketyl hydroperoxide formation	1.19×10^{12}, s^{-1}	27.9	0.2
4	$CH_3\text{–}CHO_2\text{–}CH_3 = CH_3\text{–}CH(OOH)\text{–}{}^{\cdot}CH_2$	ketyl hydroperoxide formation	3.56×10^{12}, s^{-1}	29.7	0.2
5	$OCH\text{–}CH(OOH)\text{–}CH_3 \longrightarrow CH_3\text{–}CHO + {}^{\cdot}HCO + {}^{\cdot}OH$	low-temperature chain branching	2×10^{15}, s^{-1}	43	0.2
6	$OCH\text{–}CH_2\text{–}{}^{\cdot}CH(OOH) \longrightarrow CH_2O + {}^{\cdot}CH_2\text{–}CHO + {}^{\cdot}OH$	low-temperature chain branching	2×10^{15}, s^{-1}	43	0.2
7	$CH_3\text{–}CO\text{–}CH_2(OOH) \longrightarrow CH_2O + CH_3\text{–}{}^{\cdot}CO + {}^{\cdot}OH$	low-temperature chain branching	2×10^{15}, s^{-1}	43	0.2

Note: A is the preexponential factor, X is the coefficient of variation of A, and $k = A\exp(E/RT)$.

Table 3. Sensitivity coefficients W_i before and after model optimization, calculated for the lean propane–air mixture at P = 500 atm and T = 850, 1000, and 1150 K

No.	Reaction	850 K		1000 K		1150 K	
		before optimization	after optimization	before optimization	after optimization	before optimization	after optimization
1	$^{\cdot}OH + {}^{\cdot}OH (+M) \longrightarrow H_2O_2(+M)$	0.19	0.07	0.38	0.35	0.47	0.47
2	$C_3H_8 + {}^{\cdot}HO_2 \longrightarrow {}^{\cdot}C_3H_7 + H_2O_2$	0.23	0.15	0.47	0.33	0.49	0.41
3	$^{\cdot}HO_2 + {}^{\cdot}HO_2 \longrightarrow O_2 + H_2O_2$	–0.12	–0.07	–0.26	–0.21	–0.22	–0.19
4	$^{\cdot}O_2C_3H_6OOH \longrightarrow HOOC_3H_5O + {}^{\cdot}OH$	0.29	0.16	0.43	0.28	0.16	0.2
5	$^{\cdot}C_3H_7O_2 = {}^{\cdot}CH_3–CH–CH_2(OOH)$	–0.08	–0.04	–0.22	–0.15	–0.12	–0.1
6	$^{\cdot}C_3H_7O_2 = {}^{\cdot}CH_2–CH_2–CH_2(OOH)$	0.15	0.15	0.21	0.23	0.09	0.13
7	$^{\cdot}CH_3–CHO_2–CH_3 = {}^{\cdot}CH_2–CH(OOH)–CH_3$	0.12	0.14	0.04	0.06	0.01	0.015
8	$C_4H_{10} + {}^{\cdot}OH \longrightarrow {}^{\cdot}CH_3–CH–C_2H_5 + H_2O$	0.09	0.1	0.17	0.18	0.09	0.1
9	$^{\cdot}OH + H_2O_2 \longrightarrow {}^{\cdot}HO_2 + H_2O$	–0.09	–0.04	–0.13	–0.12	–0.13	–0.11
10	$HO_2C_3H_5O \longrightarrow$ products $+ {}^{\cdot}OH$	0.12	0.19	0.02	0.06	0.001	0.007
11	$C_3H_8 + {}^{\cdot}OH \longrightarrow {}^{\cdot}CH_2–C_2H_5 + H_2O$	0.1	0.17	0.9	0.27	0.04	0.14
12	$C_3H_8 + {}^{\cdot}OH \longrightarrow {}^{\cdot}CH_3–CH–CH_3 + H_2O$	–0.004	–0.15	–0.9	–0.21	–0.07	–0.14
13	$^{\cdot}CH_2–C_2H_5 + O_2 \longrightarrow C_3H_6 + {}^{\cdot}HO_2$	–0.06	–0.08	–0.12	–0.23	–0.08	–0.21
14	$^{\cdot}CH_2–CH(OOH)–CH_3 \longrightarrow C_3H_6 + {}^{\cdot}HO_2$	–0.13	–0.06	–0.22	–0.12	–0.06	–0.03

above 200 atm, at which the discrepancy between experiment and the mechanism suggested in [17] is as large as 50–100%.

DISCUSSION

It is impossible to directly compare our experimental data with data obtained in other studies because ignition delay time depends both on the composition of the fuel mixture and on the initial pressure and temperature. At the same time, since the temperature dependence of τ is nearly Arrhenius-like (Eq. (1)), comparison is possible in terms of activation energy. Because τ still deviates from Arrhenius behavior, the uncertainty in E_a is 7 kcal/mol. In our experiment, E_a changed monotonically from 39.4 kcal/mol at a low pressure and a high temperature to 20.2 kcal/mol at a high pressure and a low temperature. Our experimental conditions are similar to those examined in an earlier study on the ignition of the $C_3H_8 : O_2 : N_2 = 2.1 : 20.6 : 77.3$ mixture [6]. Apparent activation energy in that study was 11.5–27 kcal/mol, depending on conditions, and no pressure dependence of E_a was observed.

Consider the temperature dependence of E_a for the ignition of a lean propane–air mixture, including data acquired at high diluent concentrations of >90% and $T > 1500$ K since E_a is pressure- and composition-independent under these conditions. It is demonstrated in Fig. 4 that all of the data obtained in different runs and by different authors fall close to the same fitted curve (here, the abscissa axis represents the middle points of the temperature ranges in which the activation energies are determined). Between 1000 and 1500 K, activation energy rises monotonically, increasing by 10 kcal/mol for every 100 K.

The kinetic model suggested here for propane ignition includes three different oxidation mechanisms, namely, a high-temperature ($T > 1200$ K), a low-temperature ($T < 900$ K), and an intermediate-temperature (T = 1000–1200 K) mechanism.

Above 1200 K, chain initiation is due to the dissociation of the hydrocarbon into two alkyl radicals:

$$RH \longrightarrow {}^{\cdot}R' + {}^{\cdot}R''. \qquad \text{(III)}$$

This reaction dominates over the reaction

$$RH \longrightarrow {}^{\cdot}R + {}^{\cdot}H \qquad \text{(IV)}$$

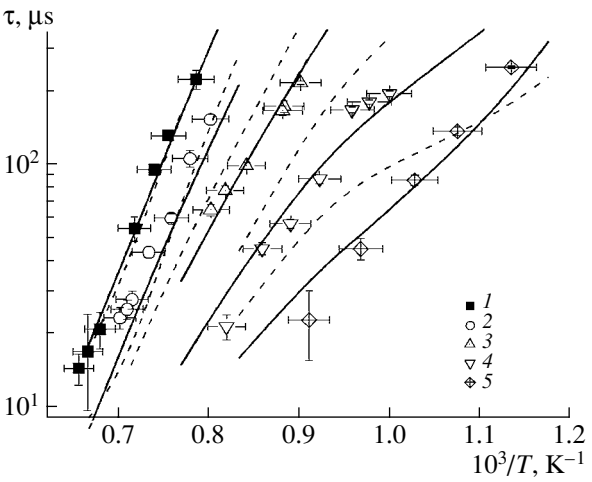

Fig. 3. Observed and calculated ignition delay time data for the propane (2%)–air mixture. The points represent experimental data, the solid lines represent data calculated using our model, and the dashed lines represent data calculated using the model suggested in [17]. P = (*1*) 4.7, (*2*) 20, (*3*) 66, (*4*) 220, and (*5*) 500 atm.

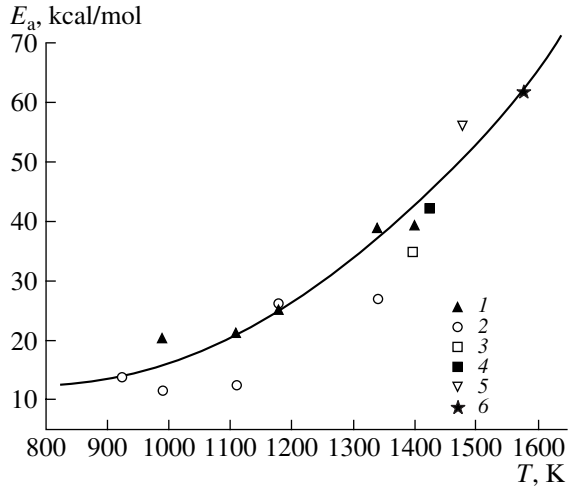

Fig. 4. Temperature dependence of the apparent activation energy of ignition for lean propane–air mixtures: (*1*) results of this study, (*2*) data from [6], (*3*) data from [3], (*4*) averaged data from [3] (φ = 0.125–2.0; T = 1250–1600 K; P = 2–10 atm; diluent concentration, 77–97%), (*5*) averaged data from [1] (φ = 0.5–1.5; T = 1375–1580 K; P = 3.5–9.7 atm; diluent concentration, 97%), and (*6*) averaged data from [5] (φ = 0.5–2.0; T = 1350–1800 K; P = 0.75–1.6 atm; diluent concentration, 78–91%).

because the activation energy of reaction (IV) exceeds by 10–15 kcal/mol the activation energy of reaction (III). Chain propagation is due to the reactions

$$RH + {}^{\cdot}OH \longrightarrow {}^{\cdot}R + H_2O, \qquad (V)$$

$$RH + {}^{\cdot}O \longrightarrow {}^{\cdot}R + {}^{\cdot}OH. \qquad (VI)$$

Reaction (V) heats the fuel mixture. The loss of free radicals is due to recombination (the reaction opposing reaction (III)).

The formation rate of radicals and, accordingly, ignition delay time are primarily determined by the branching reaction (VI); the reactions

$${}^{\cdot}H + O_2 \longrightarrow {}^{\cdot}O + {}^{\cdot}OH, \qquad (VII)$$

$${}^{\cdot}HO_2 + {}^{\cdot}CH_3 \longrightarrow {}^{\cdot}OH + {}^{\cdot}CH_3O; \qquad (VIII)$$

and the chain termination reactions

$${}^{\cdot}CH_3 + {}^{\cdot}CH_3 + M \longrightarrow C_2H_6 + M, \qquad (IX)$$

$${}^{\cdot}H + RH \longrightarrow H_2 + {}^{\cdot}R, \qquad (X)$$

$${}^{\cdot}HO_2 + {}^{\cdot}HO_2 \longrightarrow O_2 + H_2O_2. \qquad (XI)$$

In the intermediate temperature range (1000–1200 K), the main role is played by the reactions involving ${}^{\cdot}HO_2$ or H_2O_2 and chain branching is due to reaction (II) and the reaction

$$RH + {}^{\cdot}HO_2 \longrightarrow {}^{\cdot}R + H_2O_2. \qquad (XII)$$

This mechanism of ignition is illustrated by Fig. 2. Large amounts of ${}^{\cdot}HO_2$ and H_2O_2 are formed during the induction period. At the instant of ignition (dramatic increase in temperature), these species decay according to reactions (XII) and (II). As a consequence, the concentration of ${}^{\cdot}OH$ increases sharply, resulting in a temperature rise and in an increase in oxidation rate. Ignition in the intermediate temperature region is a chain process, as is indicated by the small jump of the ${}^{\cdot}HO_2$ and ${}^{\cdot}OH$ concentrations against the background of a very slow increase in temperature early in the induction period.

Below 900 K, the ignition of hydrocarbons is controlled by peroxide formation

$${}^{\cdot}R + O_2 + M \longrightarrow {}^{\cdot}RO_2 + M \qquad (XIII)$$

followed by the formation of hydroperoxides through hybridization:

$${}^{\cdot}C_3H_7O_2 = {}^{\cdot}C_3H_6O_2H. \qquad (XIV)$$

Subsequently, the alkyl hydroperoxide becomes a source of ${}^{\cdot}OH$ radicals and oxygen-containing hydrocarbons (aldehydes and ketones):

$${}^{\cdot}C_3H_6OOH + O_2 \longrightarrow {}^{\cdot}O_2C_3H_6OOH,$$

$${}^{\cdot}O_2C_3H_6OOH \longrightarrow HOOC_3H_5O + {}^{\cdot}OH, \qquad (XV)$$

$$HOOC_3H_5O \longrightarrow CH_2O + {}^{\cdot}C_2H_3O + {}^{\cdot}OH.$$

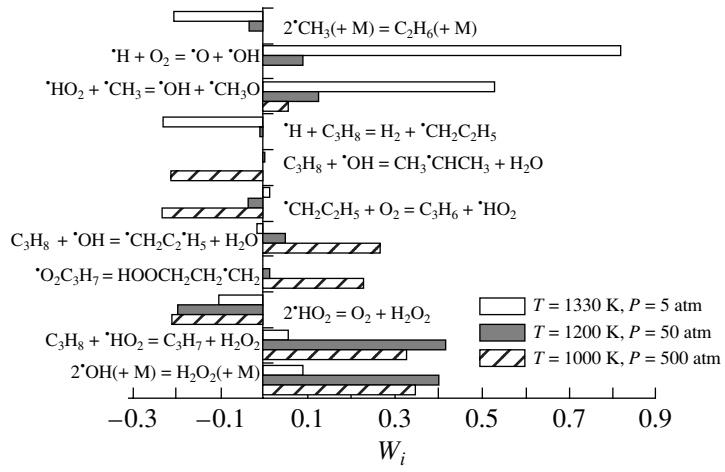

Fig. 5. Sensitivity of ignition delay time to the rate constant of the reaction for the ignition of a lean (φ = 0.5) propane–air mixture. The ignition delay time is 100 μs.

The $^{\bullet}H$ and $^{\bullet}CH_3$ radicals play an insignificant, if any, role in the low-temperature oxidation mechanism. Chain termination is due to reaction (XI) and reactions terminating alkyl peroxy radical formation:

$$C_3H_8 + {}^{\bullet}OH \longrightarrow CH_3{-}{}^{\bullet}CH{-}CH_3 + H_2O, \quad \text{(XVI)}$$

$$^{\bullet}CH_2{-}CH_2{-}CH_3 + O_2 \longrightarrow C_3H_6 + {}^{\bullet}HO_2. \quad \text{(XVII)}$$

Our kinetic model differs from other models in that its low-temperature chain branching mechanism includes reactions (XIV) and (XV).

Chain propagation rate is determined by the interplay of chain termination and initiation reactions. In the main high-temperature termination reactions, namely, the reaction opposite to (II) and reaction (IX), equilibrium depends strongly on temperature since the back reactions are characterized by high activation energies (~40 and ~90 kcal/mol, respectively). In the low-temperature mechanism, the balance of chain termination and initiation reactions is less strongly dependent on temperature.

The activation energy of the reactions opposing reactions (XVI) and (XVII) is ~20 kcal/mol. Therefore, on passing from low to high temperatures, the apparent activation energy increases considerably (Fig. 4). The temperature-induced mechanistic change is illustrated by Fig. 5.

Hydrocarbon ignition depends on the total pressure of the mixture, which contains a large amount (~78%) of a diluent (N_2 or Ar). The effect of total gas pressure on the ignition mechanism is described in our earlier publication [14]. As the pressure is raised, reaction (VII) is replaced with the reaction

$$^{\bullet}H + O_2 + M \longrightarrow {}^{\bullet}HO_2 + M. \quad \text{(XVIII)}$$

The concentration of O and H atoms during the induction period is much lower at high pressures than at low pressures. At high pressures, chain branching involving $^{\bullet}O$ and $^{\bullet}H$ through reactions (VII), (VI), and

$$^{\bullet}C_3H_7 \longrightarrow C_3H_6 + {}^{\bullet}H \quad \text{(XIX)}$$

is somewhat retarded, resulting in another mechanism of $^{\bullet}OH$ formation: at high pressures, the formation of hydroxyl radicals involves $^{\bullet}HO_2$ and H_2O_2, taking place through reactions (XVIII), (XII), (XI), and (II). Under our experimental conditions, the rates of reactions (XVIII) and (II) depend on diluent concentration and increase with increasing total pressure. It is the effect of pressure on the rate of these reactions and, accordingly, the rate of ignition that is responsible for some discrepancy between our data and data obtained at lower pressures (5–40 atm) [6].

Various processes are involved in hydrocarbon oxidation. The model considered here includes some 2500 reactions. Ignition delay time depends primarily on processes occurring early in the ignition, when the mixture temperature and the concentration of active radicals are comparatively low. The set of reactions determining the propagation of ignition differs considerably from the set of reactions responsible for the evolution of most of the energy.

CONCLUSIONS

Ignition delay time behind a reflected shock wave was measured for a lean propane–air mixture at temperatures of 880–1550 K and pressures of 2–500 atm. A detailed kinetic model is constructed, which is in good agreement with the τ data measured in the above temperature range. The apparent activation energy increases from 20 kcal/mol at T = 880–1100 K to 54 kcal/mol at T = 1270–1520 K. This increase in E_a is caused by the alteration of the mechanism of chain branching. The high E_a value at $T > 1200$ K is due to the

strong temperature dependence of the equilibrium constants of reactions (II) and (IX), which determine the concentration of $\dot{O}H$ and $\dot{C}H_3$ radicals. Below 1000 K, chain branching is degenerate and does not involve $\dot{H}$, $\dot{O}H$, or $\dot{C}H_3$ radicals. The rates of reactions (XVIII) and (II) depend on the total mixture pressure. At high total pressures, these reactions dominate over the chain branching reactions involving O and H atoms (reactions (VIII), (VI), and (XIX)). It is the pressure dependence of the branching rate that is responsible for the difference between our E_a data (~20 kcal/mol at P = 200–500 atm) and the E_a data obtained by other researchers (~13 kcal/mol at P = 10–40 atm [6]).

REFERENCES

1. Lamoureux, N., Paillard, C.-E., and Vaslier, V., *Shock Waves*, 2002, vol. 11, p. 309.
2. Davidson, D.F., Herbon, J.T., Horning, D.C., and Hanson, R.K., *Int. J. Chem. Kinet.*, 2001, vol. 33, p. 775.
3. Burcat, A., Lifshitz, A., Scheller, K., and Skinner, G.B., *Proc. 13th Symp. on Combustion*, 1971, p. 745.
4. Thomas, G.O. and Brown, C.J., *Combust. Flame*, 1999, vol. 117, p. 861.
5. Kilyoung Kim and Kuan Soo Shin, *Korean Chem. Soc.*, 2001, vol. 22, p. 303.
6. Cadman, P., Thomas, G.O., and Butler, P., *Phys. Chem. Chem. Phys.*, December 7, 2000, p. 5411.
7. Horning, D.C., Davidson, D.F., and Hanson, R.K., *J. Propul. Power*, 2002, vol. 18, p. 363.
8. Koert, D.N., Pitz, W.J., Bozelli, J.W., and Cernansky, N.P., *27th Symp. on Combustion*, Pittsburgh: Combustion Inst., 1999, p. 633.
9. Konnov, A.A., *28th Symp. on Combustion*, Edinburgh, 2000, p. 317.
10. Dagaut, P., Luche, J., and Cathonnet, M., *Fuel*, 2001, vol. 80, p. 979.
11. Peterson, E.L., Davidson, D.F., Rohrig, M., Hanson, R.K., and Bowman C.T, *J. Propul. Power*, 1999, vol. 15, p. 82.
12. Peterson, E.L., Davidson, D.F., and Hanson, R.K., *Combust. Flame*, 1999, vol. 117, p. 272.
13. Frenklach, M., Wang, H., Yu, C.-L., Goldenberg, M., Bowman, C.T., Hanson, R.K., Davidson, D.F., Chang, E.J., Smith, G.P., Golden, D.M., Gardiner, W.C., and Lissianski, V., *Gas Research Institute Topical Report no. GRT-9570058*, 1995.
14. Zhukov, V.P., Sechenov, V.A., and Starikovskii, A.Yu., *Fiz. Goreniya Vzryva*, 2003, vol. 39, no. 5, p. 3.
15. Vozhenkov, S., Starikovskaia, S., Seshenov, V., Starikovskii, A., and Zhukov, V., *Rroc. 41st ATAA Aerospase Sciences Meeting and Exhibition*, Reno, Nevada, USA, 2003, ATAA-2003-0876.
16. Zhukov, V.P., Sechenov, V.A., and Starikovskii A.Yu., *Combust. Flame*, 2005, vol. 140, p. 196.
17. Curran, H.J., Gaffuri, P., Pitz, W.J., and Westbrook, C.K., *Combust. Flame*, 1998, vol. 114, p. 149.
18. Curran, H.J., Gaffuri, P., Pitz, W.J., and Westbrook, C.K., *Combust. Flame*, 2002, vol. 129, p. 253.
19. Ciezki, H.K. and Adomeit, G., *Combust. Flame*, 1993, vol. 93, p. 421.
20. Fieweger, K., Blimenthal, R., and Adoineit, G., *Combust. Flame*, 1997, vol. 109, p. 599.
21. Bowman, C.T., Hanson, R.K., Davidson, D.F., Gardiner, W.C., Jr., Lissianski, V., Smith, G.P., Golden, D.M., Frenklarh, M., and Goldenberg M., http://www.me.berkeley.edu / gri-mech/.
22. Smith, G.R., Golden, D.M., Frenldach, M., Moriarty, N.W., Eiteneer, B., Goldenberg, M., Bowman, S.T., Hanson, R.K., Song, S., Gardiner, W.C., Lissianski, V.V., and Qin, Z., http://www.me.berkeley.edu / gri-mech/.
23. Stupochenko, E.V., Losev, S.A., and Osipov, A.I., *Relaksatsionnye protsessy v udarnykh volnakh* (Relaxation Processes in Shock Waves), Moscow: Nauka, 1965.
24. Bhaskaran, R.F. and Roth, P., *Prog. Energy Combust. Sci.*, 2002, vol. 28, p. 151.
25. Starikovskii, A.Yu., *Khim. Fiz.*, 1993, vol. 12, no. 5, p. 645.
26. Petersen, E.L. and Hanson, R.K., *Shock Waves*, 2001, vol. 10, p. 405.
27. Luts, A.E., Lee, R.K., and Miller, J.A., *SENKIN: A FORTRAN Program for Predicting Homogeneous Gas-Phase Chemical Kinetics with Sensitivity Analysis*, Livermore: Sandia National Laboratories, 1989, report no. SANDTA89-8009.